Ore Geology Reviews 134 (2021) 104169

Contents lists available at ScienceDirect

Ore Geology Reviews

journal homepage: www.elsevier.com/locate/oregeorev

Resource estimation of the sulfide-rich deposits of the Yuhuang-1 hydrothermal field on the ultraslow-spreading Southwest Indian Ridge

Junyu Yu [a,b], Chunhui Tao [a,b,d,*], Shili Liao [b], Ágata Alveirinho Dias [c,e], Jin Liang [b], Weifang Yang [b], Chuanwei Zhu [f]

[a] Ocean Collage, Zhejiang University, Zhoushan 316021, Zhejiang, China
[b] Key Laboratory of Submarine Geosciences, Second Institute of Oceanography, Ministry of Natural Resources, Hangzhou 310012, China
[c] Institute of Science and Environment, University of Saint Joseph, Macao SAR, China
[d] School of Oceanography, Shanghai Jiaotong University, Shanghai 200030, China
[e] Instituto Don Luiz, Faculty of Sciences, University of Lisbon, Portugal
[f] Institute of Geochemistry, Chinese Academy of Sciences, State Key Laboratory of Ore Deposit Geochemistry, Guiyang 550002, Guizhou, China

ARTICLE INFO

Keywords:
Seafloor massive sulfide deposits
Resource estimate
Yuhuang-1 hydrothermal field
Southwest Indian Ridge

ABSTRACT

Seafloor massive sulfide (SMS) deposits are important deep-sea mineral resources expected to occur predominantly on slow- and ultraslow-spreading mid-ocean ridges. Resource estimates are already available for some of the largest SMS deposits on slow-spreading ridges but not on ultraslow-spreading ridges. Based on geological mapping and sampling, this study investigates the distribution and content of sulfide-rich deposits in the Yuhuang-1 hydrothermal field (YHF), located on the ultraslow-spreading Southwest Indian Ridge. The sulfide-rich deposits in the YHF are composed of two areas ~500 m apart: the southwest sulfide area (SWS) and the northeast sulfide area (NES). We calculated the volume of sulfide-rich moundsin the YHF and arrived at a total accumulation of ~10.6×10^6 tons, including at least ~7.5×10^5 tons of copper and zinc and ~18 tons of gold. Furthermore, considering the coverage of layered hydrothermal sediment mixed with sulfide-rich breccias, which may have underlying massive sulfide deposits, the maximum total mass was estimated at ~45.1×10^6 tons. This suggests that the YHF is one of the largest SMS deposits worldwide and confirm that ultraslow-spreading ridges have the greatest potential to form large-scale SMS deposits.

1. Introduction

Since the first observation of a "black smoker" at the 21°N, East Pacific Rise in 1979 (Spiess et al., 1980), seafloor hydrothermal activity and its associated polymetallic sulfides, which are important potential mineral resources, have attracted extensive attention from the international community and scientists (e.g., Baker and German, 2004; Beaulieu et al., 2015; Hannington et al., 2010; Lusty and Murton, 2018; Petersen et al., 2016). Statistically, the total accumulation of seafloor sulfide deposits in submarine neovolcanic zones in the global oceans is up to ~6×10^8 tons; and the tonnage of sulfides on slow- and ultraslow-spreading (spreading rate <40 mm/yr) centers accounts for ~86% of the total mass of sulfide deposits at ridges (Hannington et al., 2011). For several hydrothermal fields located on slow-spreading ridges, studies of the distribution of sulfide deposits and estimates of their potential resource have already confirmed that the large-scale of sulfide reserves on this type of ridge system (e.g. Trans-Atlantic Geotraverse, TAG, hydrothermal field on the Mid-Atlantic Ridge, MAR; German et al., 2016; Hannington et al., 2011, 1998; Murton et al., 2019).

Ultraslow-spreading ridges, with spreading rates of less than ~20 mm/yr, are characterized by stable tectonic environments, deep hydrothermal circulation, and large-scale water–rock reactions (Dick et al., 2003; German et al., 2016), which should lead to the formation of the largest SMS deposits. To date, >20 hydrothermal fields have been discovered and confirmed on ultraslow-spreading ridges (data from www.vents-data.interridge.org/). Among them, however, only for Mount Jourdanne deposit on the Southwest Indian Ridge (SWIR) size was reported, and estimated at <3000 tons using the area vs. tonnage relationship for the Solwara-1 deposit as a reference (Hannington et al., 2010, 2011), which is much smaller than expected. Therefore, there is currently still a lack of studies characterizing the distribution and content of large sulfide resources on ultraslow-spreading ridges.

* Corresponding author at: Key Laboratory of Submarine Geosciences, Second Institute of Oceanography, Ministry of Natural Resources, Hangzhou 310012, China.
E-mail addresses: taochunhuimail@163.com, taochunhui@sio.org.cn (C. Tao).

https://doi.org/10.1016/j.oregeorev.2021.104169
Received 22 July 2020; Received in revised form 4 February 2021; Accepted 14 April 2021
Available online 17 April 2021

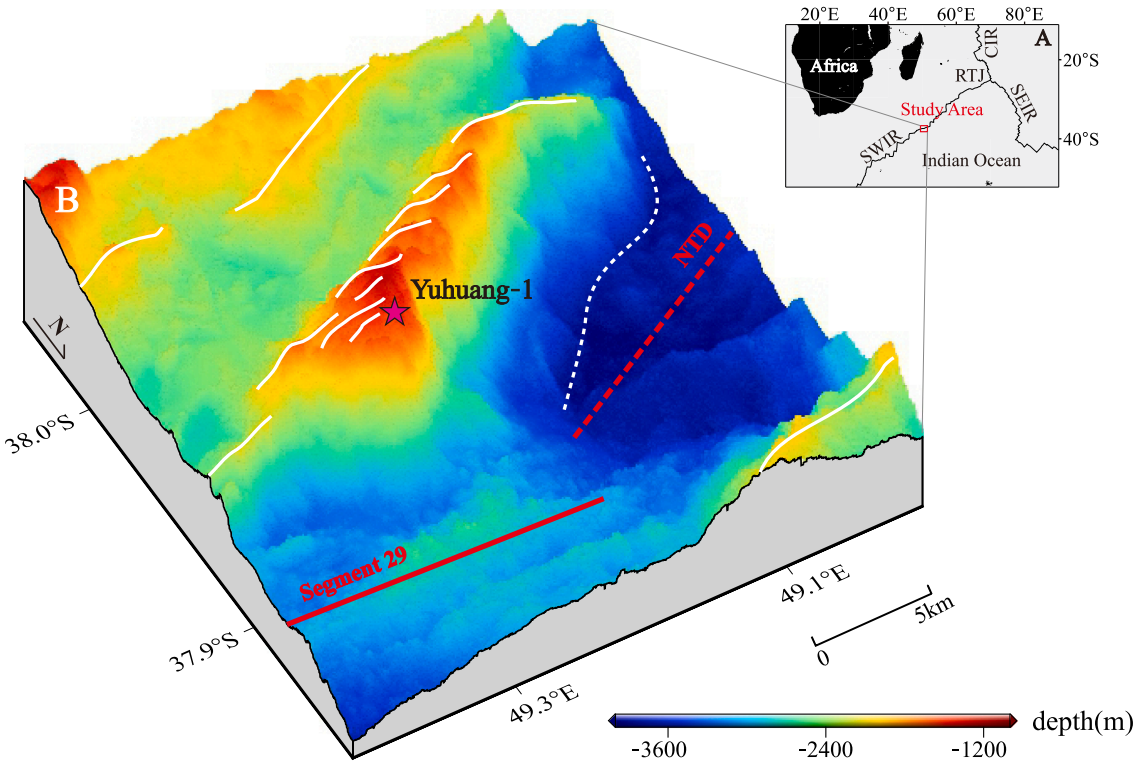

Fig. 1. (A) Location of the YHF on the SWIR; and (B) a high-resolution bathymetry map showing an oblique view from the axial volcanic ridge. The ridge segment and non-transform discontinuity (NTD) were obtained from Cannant et al. (1999) and Sauter et al. (2001). The white lines show a series of NE-NWW-striking faults and the white dotted line shows the inferred termination of the detachment fault according to Liao et al. (2018a).

The Yuhuang-1 hydrothermal field (YHF) on the ultraslow-spreading SWIR was first reported in the DY21 cruise. Thence, the DY34, 39, 40, 43 and 58 cruises were conducted in this field to obtain estimates of the sulfide distribution and thickness using a deep-tow camera, TV-grab sampling, and self-potential surveys (Tao et al., 2014; Liao et al., 2018a; Zhu et al., 2020b). Photos and videos of the substrate were obtained, together with sulfide samples and self-potential anomalies, providing first-hand data to investigate the sulfide distribution and estimate the total resources of the YHF.

In this work, we calculated the sulfide resources for different areas of the YHF and studied the mineralization and content of selected samples from sulfide deposits, mineralized rocks, and hydrothermal sediments. Based on this integrative analysis, a preliminary estimate of the size and tonnage of the sulfide deposits and metal contents in the YHF is presented, providing a basis for sulfide exploration on the SWIR.

2. Geological background

The SWIR forms the boundary between the African Plate and the Antarctic Plate, running from the Rodrigues Triple Junction (RTJ) in the east, to the Bouvet Triple Junction (BTJ) in the west (Fig. 1A), with a total length of approximately 8000 km (Georgen et al., 2001; Tao et al., 2014). It is an ultraslow-spreading mid-ocean ridge, with a full spreading rate of 14–16 mm/yr (Dick et al., 2003). The axial rift valley of the SWIR is divided into several segments by a series of north–south transform faults. The local magma supply and suitable crustal permeability play key roles in hydrothermal activities (Tao et al., 2012, 2014), although the source of the magma is still controversial (Georgen et al., 2001; Sauter et al., 2001; Li et al., 2015; Yu and Dick, 2019).

The YHF (49.26°E, 37.94°S) is located on Segment 29 of the SWIR, between the Indomed (46.0°E) and Gallieni (52.2°E) transform faults (Cannat et al., 1999, 2006; Sauter et al., 2001). This segment shows asymmetric spreading features, and a series of NE-NWW-striking faults has developed in the highland region. This site is located near the top of the off-axis slope on the south rift wall, approximately 7–8 km from the ridge axis at a water depth of 1400–1900 m (Fig. 1B). No significant temperature or turbidity anomalies were detected, indicating that the YHF is likely an inactive field (Tao et al., 2014). The sampling of ultramafic rocks, together with the development of detachment faults, suggests that those faults and the associated mantle exposure may control the hydrothermal activity in this field (Zhu et al., 2020a; Liao et al., 2018a).

3. Methods

3.1. Geological survey

The sulfide distribution of the YHF was studied via an interpretation of photos and videos obtained from six comprehensive towed survey lines performed during the DY30 and DY34 cruises. The interval between the survey lines was approximately 300 m, and an ultra-short baseline (USBL) was used to control the positioning accuracy within ±5 m. During the survey, the sulfide distribution was also verified via TV-grab sampling and shallow drilling by a robotic lander-type seafloor drilling rig in different sulfide distribution areas (Fig. 2A). Six cruises included 13 sampling stations using a TV-grab and 15 stations using a lander-type drilling rig were operated by the RVs “Dayangyihao” and “Xiangyanghong 10” (Table 1).

3.2. Bulk geochemical analysis

The bulk geochemistry of the sediment and core samples was analyzed at the Australia Laboratory Service (ALS) in Guangzhou, China. The major elements were analyzed using PANalytical PW2424 X-ray fluorescence spectrometry. The standard samples were GBW07105, NCSDC47009, and SARM-4, resulting in the data errors being within 5%. The trace elements were analyzed using an Agilent 7700x ICP-MS, and the reference samples GBM908-10 and MRGeo08 were used to

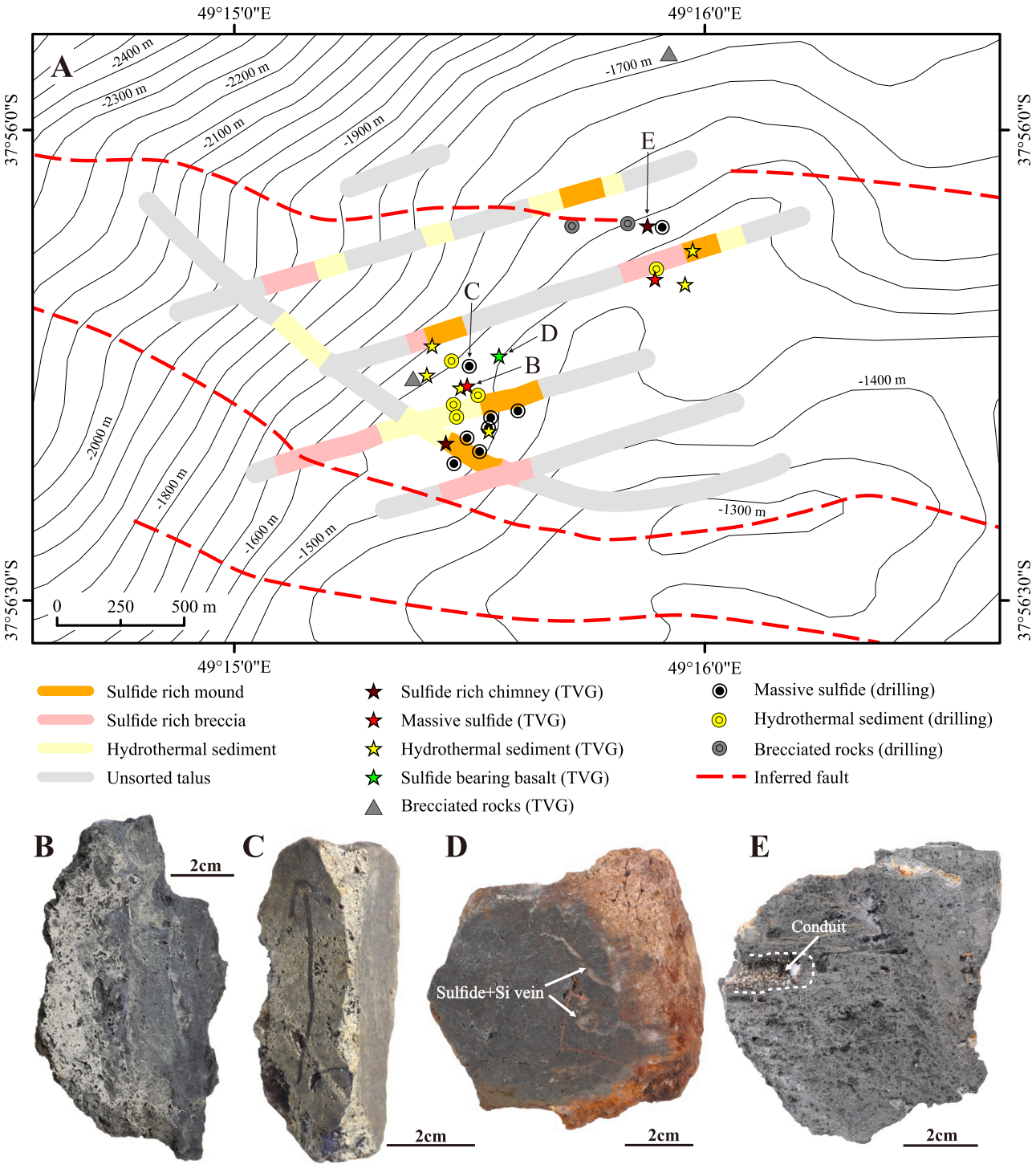

Fig. 2. (A) A map of the survey lines and sampling stations, with photographs of the sulfide-rich samples obtained from the YHF. The locations of samples (B)–(E) are indicated in (A) with arrows; (B) a pyritic massive sulfide, from 34TVG22; (C) a drilling core sample of a Cu-rich massive sulfide, from 43MDD04; (D) a basaltic sample with sulfide-bearing vein, from 39TVG04; and (E) sulfide-rich chimney debris containing a fluid conduit, from 34TVG23.

control the data quality to an error of <10%.

4. Results

4.1. Sulfide-rich areas and host rocks of the YHF

Two main sulfide-rich areas, ~500 m apart, were identified in the YHF: (1) the southwest sulfide area (SWS) and (2) the northeast sulfide area (NES; Fig. 3A). The area of the SWS is ~48.5 × 10^4 m^2, while the NES covering a relatively small area ~13.4 × 10^4 m^2. No active vents or vent-endemic species were observed in either area.

4.1.1. Southwest sulfide area (SWS)

The substrate found in the SWS can be divided into three types: sulfide-rich mounds, sulfide-rich breccias, and hydrothermal sediments. No upright sulfide chimneys were discovered in this area, and only oxidized relict chimneys were observed on the sulfide-rich mounds (Fig. 3B). Moreover, the sulfides exposed on the seafloor are extensively

Table 1
Information of the samples from the SWS, NES, and host rocks of the YHF. Length represents the length of the drilling core.

Area	Station	Sampling methods	Longitude (°E)	Latitude (°S)	Depth (m)	Length (m)	Comment
SWS	34TVG22	TV-grab	49.258	37.942	1499	–	Sulfide-rich breccia, oxide crusts, and hydrothermal sediments
	39TVG04	TV-grab	49.259	37.941	1505	–	Sulfide-bearing basalt, opal, and altered basalt
	39TVG05	TV-grab	49.257	37.941	1622	–	Hydrothermal sediments, Opal, intensive altered basalt
	40TVG14	TV-grab	49.258	37.942	1527	–	Basalt and hydrothermal sediment
	40TVG17	TV-grab	49.257	37.942	1539	–	Hydrothermal sediments, ultramafic rock
	58TVG17	TV-grab	49.259	37.943	1522	–	Sulfide-rich chimney debris
	58TVG18	TV-grab	49.258	37.944	1518	–	Massive sulfide
	39MDD02-1	Drilling rig	49.259	37.944	1436	2.0	Massive sulfide and hydrothermal sediment
	39MDD02-2	Drilling rig	49.258	37.943	1514	1.6	Sediments and altered basalt
	39MDD01	Drilling rig	49.258	37.942	1656	3.8	Sediments and basaltic rubble
	39MDD02	Drilling rig	49.259	37.944	1533	7.6	Massive sulfide and hydrothermal sediment
	43MDD01	Drilling rig	49.260	37.943	1506	8.0	Massive sulfide and hydrothermal sediment
	43MDD02A	Drilling rig	49.258	37.943	1513	3.8	Sediments and basaltic rubble
	43MDD02B	Drilling rig	49.259	37.945	1522	9.0	Massive sulfide and hydrothermal sediment
	43MDD03	Drilling rig	49.259	37.943	1501	1.9	Sediments and basaltic rubble
	43MDD04	Drilling rig	49.258	37.942	1532	8.5	Massive sulfide and hydrothermal sediment
	58MDD03	Drilling rig	49.258	37.944	1520	0.8	Massive sulfide
	58MDD06	Drilling rig	49.258	37.945	1535	4.4	Massive sulfide
NES	21TVG22	TV-grab	49.265	37.939	1443	–	Sulfide-rich breccia
	34TVG23	TV-grab	49.265	37.937	1557	–	Sulfide-rich chimney, sulfide-rich breccia
	34TVG24	TV-grab	49.266	37.938	1494	–	Hydrothermal sediment and altered basalt
	40TVG15	TV-grab	49.266	37.939	1471	–	Hydrothermal sediment
	39MDD03	Drilling rig	49.265	37.938	1487	1.7	Hydrothermal sediment and altered basalt
	43MDD05	Drilling rig	49.265	37.937	1521	0.9	Sulfide-bearing basalt
Host rocks	40TVG16	TV-grab	49.256	37.942	1547	–	Altered basalt and serpentinized ultramafic rock
	21TVG20	TV-grab	49.265	37.931	1698	–	Basalt and serpentine
	43MDD06A	Drilling rig	49.264	37.937	1564	1.2	Altered basalt
	43MDD06B	Drilling rig	49.262	37.937	1581	4.0	Altered basalt

oxidized to a red-brown color and collapse structures of sulfides occur frequently throughout the entire zone (Fig. 3C). The area can be further divided into seven different sub-regions. Two sulfide-rich mounds with an area of ~11.5 × 10^4 m^2 (~24% of the total area), primarily distributed in the middle and southeast regions. The southeast mound is the larger of the two, with an area of ~10.9 × 10^4 m^2, exposing mainly oxidized sulfide deposits (Fig. 3B and 3C). The samples collected on the mounds can be classified into three types, based on the main metal minerals: (1) Fe-rich sulfide deposits (Fig. 2B); (2) Zn-rich sulfide deposits; and (3) Cu-rich massive sulfide deposits (Fig. 2C). Details of the samples (1) and (2) were described previously (Liao et al., 2019a); they are mainly composed of sphalerite, pyrite, and amorphous silica, with minor amounts of marcasite and chalcopyrite. Samples (3) contained >60% of chalcopyrite in the whole ore, showing a grid structure coexisting with isocubanite. In addition, debris from sulfide-bearing basalts (Fig. 2D) with sulfides filling the pores and cracks were also observed on the edge of the larger mound. This debris likely corresponds to the stockwork that was exposed on the surface due to the presence of tectonic faults in this area.

In addition to the two sulfide-rich mound regions, there are three sulfide-rich breccia regions with a total area of ~12.8 × 10^4 m^2 that contain breccia- or rubble-like hydrothermal products. These are scattered in the direction of lower topography, with the mounds at the center, suggesting that these sulfide-rich breccias were formed by sliding and accumulation in the low-lying region after the collapse of sulfide chimneys or mounds; many of these regions have been covered by pelagic sediments (Fig. 3D). In addition, two hydrothermal sediments regions with about half of the total area, characterized by pelagic ooze sediments with variable hydrothermal precipitates and host-rock debris, are distributed on the flat terrain of the SWS. In some regions, as verified by shallow drilling results, the hydrothermal sediments cover sulfide-rich deposits (thicknesses of 0.5–1 m) that show red-brown colors, providing evidence of highly oxidized sulfide content (Fig. 3E; samples 39TVG05, 40TVG14, and 40TVG17).

4.1.2. Northeast sulfide area (NES)

The substrate in the NES is similar to that observed in the SWS. The northwestern, central, and southeastern parts of the NES present three similar sulfide-rich mounds, with a total area of ~2 × 10^4 m^2. The mounds show red-brownish massive sulfide deposits, sporadically overlaid by hydrothermal sediments. Here, in-situ inactive chimneys were observed isolated on the basement (Fig. 3F). The area of the chimneys is approximately 20 m × 20 m. The fact that no active chimneys were found, suggests that the hydrothermal activity has likely ceased. Based on the survey observations, the chimneys' height ranged between 1 and 2 m. The collected chimney (sample 34TVG23; Fig. 2E) had a height of ~50–60 cm, showing a sulfide-rich mineralogy and well-defined fluid conduits.

In the southern region of the NES, an area of ~2.3 × 10^4 m^2 was found to have a distribution of red-brown sulfide-rich breccias, part of which were covered by hydrothermal sediments. This region lies between two mounds but is not as large as the SWS. A sulfide-rich deposit sample (21TVG22) was obtained in this region. Based on the mineralogical studies (Liao et al., 2018a, 2019a), the sulfide sample mainly contains sphalerite, pyrite, chalcopyrite, marcasite, pyrrhotite, isocubanite, and amorphous silicon. Here, hydrothermal sediments (gray-yellow ooze with variable amounts of hydrothermal precipitates and host-rock debris) also cover the flattest topography, with an area of ~9.2 × 10^4 m^2 (~69% of the total area; samples 34TVG24 and 40TVG15).

4.1.3. Host rocks

Talus coated with a yellow–brown oxidation layer was observed around the YHF sulfide area (Fig. 3G). Two type of brecciated rocks were collected: the first sample (40TVG16) was obtained near the SWS, with a size of 22 cm × 18 cm × 16 cm, and it was mainly composed of fragments of serpentinized pyroxenite cut by small serpentine veins; the other sample (21TVG20) was collected near the NES, with a size of 4 cm × 2.5 cm × 2 cm, and containing both basaltic and ultramafic fragments.

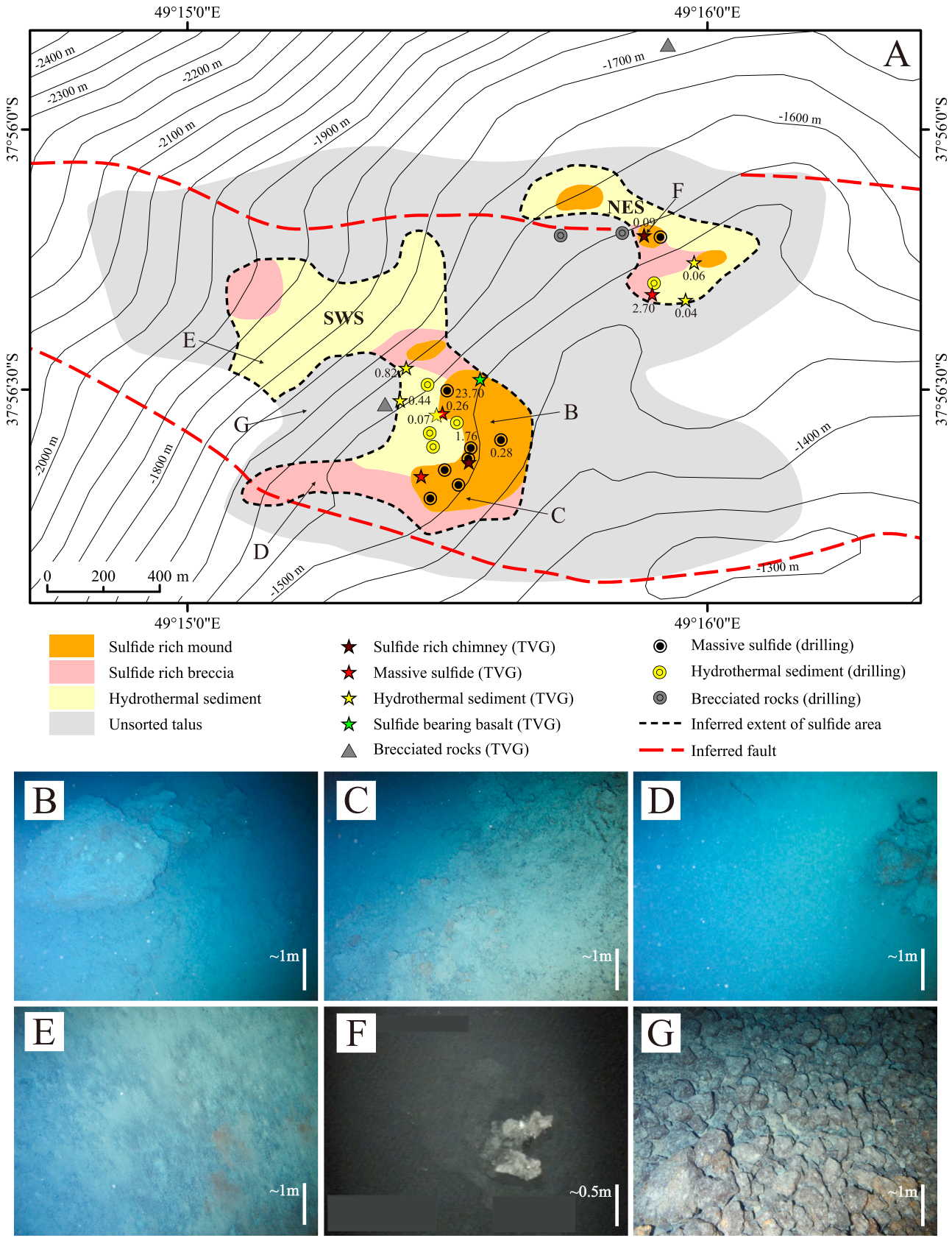

Fig. 3. (A) A geological map of the YHF based on high-resolution bathymetry, video surveys, and sampling. The colored areas are based on survey observations. The numbers adjacent to the sampling stations indicate the grade of Cu (wt.%) of the corresponding sulfide-rich deposits. The locations of photos (B)–(G) are indicated in (A) with arrows; (B) weathered sulfide-rich chimney debris; (C) a sulfide-rich mound with a degree of slope in the SWS; (D) sulfide-rich breccia covered by sediments; (E) red-brownish hydrothermal sediment; (F) an inactive sulfide chimney approximately 1–2 m high observed by the camera when performing TV-grab sampling (34TVG23); (G) yellow-brownish unsorted talus.

Table 2
Composition of sulfide-rich deposits obtained from the YHF. Data for core samples and hydrothermal sediment are from this study, and data for the massive sulfides of surface samples are obtained from Liao et al. (2018a). "n" represents the number of samples; subseafloor samples were taken separately from 3 drilling stations (39MDD02, 43MDD01, 43MDD04) at different depths.

Area	Sample type	n	Fe (wt. %)	Cu (wt. %)	Zn (wt. %)	Au (μg/g)	Ag (μg/g)
SWS	Sulfide-rich samples (including surface and core samples)	41	25.14	3.83	6.78	2.87	22.86
	Hydrothermal sediment	3	7.89	0.44	0.08	0.12	0.09
NES	Sulfide-rich samples (surface)	4	24.69	2.05	20.75	2.65	76.28
	Hydrothermal sediment	2	1.34	0.05	0.01	0.01	0.07
Total	All of the sulfide-rich samples	45	24.98	3.18	11.86	2.76	42.28

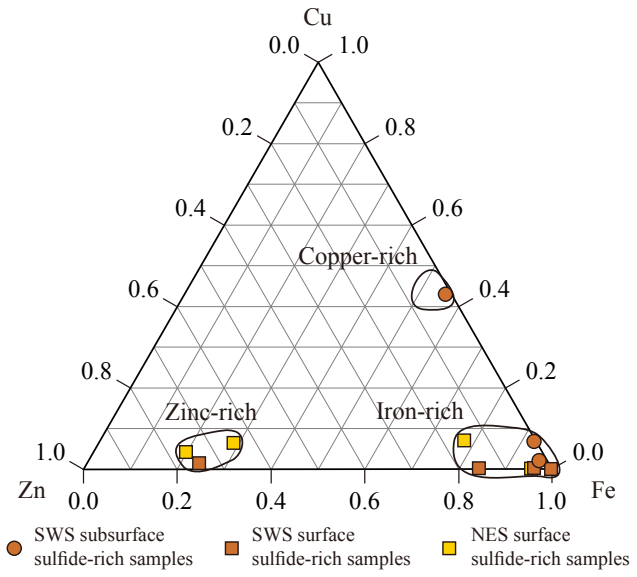

Fig. 4. Cu–Fe–Zn classification of the sulfide-rich samples in the YHF.

4.2. Composition of sulfide-rich deposits

The copper (Cu), zinc (Zn), iron (Fe), and precious-metal (gold, Au and silver, Ag) contents of the hydrothermal deposits are distinct in the SWS and NES areas (Table 2). Based on the major ore-forming element content, the YHF sulfide deposits can be classified in general as Cu-rich, Zn-rich, or Fe-rich types (Fig. 4). Samples of sulfide-rich deposits were collected from the interiors of the hydrothermal mounds (using drilling to reach the subsurface) and from the surface (using TV-grabs). In the SWS, the subsurface deposits revealed an average Cu and Zn content of 8.58 wt% and 0.39 wt%, respectively. Samples collected at the surface are, in turn, Zn-rich, showing an average Zn content of 11.61 wt%, and an average Cu content of 0.26 wt%. The average Fe content of the subsurface and surface samples is relatively similar, with 27.19 wt% and 22.41 wt%, respectively. In the NES, the average contents of the surface sulfide-rich deposits were 2.05 wt% for Cu and 20.75 wt% for Zn. The average Au content was similar in the two areas at 2.65 μg/g and 2.87 μg/g, respectively. The Cu content of the hydrothermal sediments from the SWS reached 0.44 wt%, while that of the NES was relatively low, 0.05 wt% on average.

5. Discussion

5.1. Distribution of sulfide-rich deposits and host rocks

The substrate around the YHF is dominated by basalts and altered ultramafic rocks covered by a layer of brecciated rocks (ultramafic and basaltic), which may have been formed, based on their morphology, by tectonic activity at the seafloor (e.g., sample 40TVG16 and 21TVG20). This is similar to what has been described for other tectonic-hosted deposits (e.g., the Logatchev-1 and Rainbow hydrothermal fields, MAR, and the Longqi-1 hydrothermal field, SWIR) controlled by detachment faults (Fouquet et al., 2010; Marques et al., 2006; Petersen et al., 2009; Tao et al., 2020). However, it differs from observations of magmatic-hosted deposits (e.g., the Lilliput hydrothermal field, MAR), which are dominated by eruptive lava flows (Haase et al., 2009). The YHF is a tectonic-hosted field where the metals in its deposits are mainly derived from mafic and ultramafic host rocks.

Collapsed relict chimneys were observed on the SWS mounds (Fig. 3B), which may be related to increasing structural instability as the chimneys grow taller, dissolution of thermodynamically unstable minerals (e.g., anhydrite, CaSO4), and ground motions caused by geotectonic instabilities. In addition, large sulfide-rich debris is a common feature entrained in sediments on the flanks of the mounds (e.g., Fig. 3D), similar to what has been described for extinct SMS (eSMS) mounds observed in the TAG hydrothermal field (Murton et al., 2019). In addition, the SWS sulfides were formed through multi-stage mineralization (Liao et al., 2018a, 2019a), which may be due to the accumulation of sulfides from different mineralization stages during long periods of seafloor weathering and destruction following the extinction of the hydrothermal activity in the mounds. Due to the extensive collapse and oxidation, the sulfide distribution area of the SWS is relatively large, but it may be thinner now than when there was activity. Upright chimney relicts were discovered in the middle of the NES mound (Fig. 3F), suggesting that the sulfide structure has not been completely damaged and that the morphology of the mounds is likely to be similar to that of an active mound. The lack of active chimneys, extensive collapse and oxidation, and the absence of vent biological communities, provide reliable indications of hydrothermal inactivity in the YHF.

5.2. Resource estimate of the YHF

To estimate the resources of the SMS deposits, the volume of the ore body needs to be calculated first. Hannington et al. (1998) used the method of summing the volumes of the blocks, using the base area multiplied by the thickness ($V = S \times h$). However, this method requires extensive and detailed deep-drilling cores to divide the mound into blocks. Due to the limitations of the drilling technology, the details of the morphology and grade with depth in the YHF have not yet been obtained. Even though the SMS deposits vary in different geological backgrounds, they generally have a distinct conical shape (Fouquet et al., 2010). For example, 17 drilling cores in the TAG active mound from the ODP158 cruise identified the mound as a cone, with an underlying inverted cone as the stockwork zone (Humphris et al., 1995). The Bent Hill massive sulfide deposit in the Middle Valley, which was found in the drilling results of the ODP139 and ODP169 cruises, showed a morphology composed of two opposing cones sharing a base covered by a thick layer of sediment (Zierenberg et al., 1998). Therefore, the conical volume ($V = 1/3\ S \times h$) was used to calculate the mound volumes in this study.

The thickness of the mounds in the SWS is at least 65 m, based on the inversion result from self-potential exploration (Zhu et al., 2020b). Because of the geological background, the sulfide distribution and the diameter of the outcrop (~200 m) are similar to those of the TAG active mound; the thickness of the mounds in the NES was initially set to 45 m based on the Ocean Drilling Program (ODP) results (Hannington et al.,

Table 3
Estimated masses of sulfides and metals for the YHF. The bulk-density data are obtained from Tao et al. (2013). The thickness of the NES is based on the TAG active mound (Hannington et al., 1998), whereas that of the SWS is an inversion result from the self-potential data obtained from Zhu et al. (2020b). The thickness of hydrothermal sediment is based on Liao et al. (2018a). The grade data are presented in Table 2. The estimated total tonnage for the YHF assumes that the stockwork zone accounts for approximately 30% of the mineralization (Hannington et al., 1998). The outcrop area is calculated using ArcGIS, and the reference coordinate system is GCS_WGS_1984.

Area	Type	Outcrop Area (m^2)	Thickness (m)	Volume (m^3)	Bulk Density (g/cm^3)		Mass (Mt)		Cu (t)	Zn (t)	Au (t)
					Saturation	Dry	Saturation	Dry			
SWS	Sulfide-rich mound	115,275	65	2,497,625	2.525	2.19	6.31	5.47	209,259	372,132	15.70
	Sulfide-rich breccia	128,067	0.5	64,034			0.16	0.14	5365	9541	0.40
	Hydrothermal sediment	241,171	0.5	120,586	1.3		0.16		696	119	0.02
	Total of SWS	484,513		2,682,244			6.62	5.61	215,320	381,792	16.12
NES	Sulfide-rich mound	19,542	45	293,130	2.525	2.19	0.74	0.64	13,160	133,206	1.70
	Sulfide-rich breccia	22,550	0.5	11,275			0.03	0.02	506	5124	0.07
	Hydrothermal sediment	92,401	0.5	46,201	1.3		0.06		29	4	0.001
	Total of NES	134,493		350,606			0.83	0.67	13,695	138,333	1.77
Total		619,006		3,032,850			7.45	6.28	229,015	520,125	17.89
Total including the stockwork zone							10.65	8.97			

1998; Tivey et al., 1995). The sulfide bulk density refers to the average value of the surface sulfide samples in the SWIR; that is, the wet density is 2.525 g/cm^3 and dry density is 2.19 g/cm^3 (Tao et al., 2013). However, the high porosity of the surface samples reduces the density, so the bulk density of the whole deposit may be >3 g/cm^3 (Spagnoli et al., 2016; Jamieson et al., 2014; Graber et al., 2020).

Except for the massive sulfide deposits in the mounds, the YHF is generally covered by a layer of hydrothermal sediments. The average Cu content in the SWS and NES can reach up to 0.44 wt% and 0.05 wt% respectively; values that are significantly higher than those of the Saldanha hydrothermal field (Dias and Barriga, 2006), the Dragon Horn area (Liao et al., 2018b), and the Duanqiao-1 hydrothermal field (Liao et al., 2019b) but which are close to that of the Atlantis-II-Deep deposit (Guney et al., 1988). The thicknesses of the hydrothermal sediment and the sulfide-rich breccia areas were estimated to be 0.5 m (Liao et al., 2018a). The density of the hydrothermal sediment was initially set to 1.3 g/cm^3 (Yu et al., 2011). The grades of the different samples are listed in Table 2. The formulas used in the resource estimate are as follows:

$V_1\ [m^3] = 1/3 \times S\ [m^2] \times h\ [m]$; $V_2\ [m^3] = S\ [m^2] \times h\ [m]$,

$M\ [t] = V\ [m^3] \times \rho\ [g/cm^3]$; Total $M\ [t] = \Sigma M_{1,\ 2,\ 3\ldots}[t]$,

where V_1 is the volume of the sulfide-rich mound, V_2 is the volume of the sulfide-rich breccia and hydrothermal sediment, ρ is the bulk density of the sulfide-rich deposits, and M is the mass.

The total wet weight of the sulfide-rich deposits in the SWS was calculated to be $\sim 6.6 \times 10^6$ tons, while the mass of Cu and Zn reached $\sim 6 \times 10^5$ tons, with an additional ~16 tons of Au. The total tonnage in the NES is relatively small, with a wet weight of $\sim 8.3 \times 10^5$ tons, including $\sim 1.5 \times 10^5$ tons of copper and zinc and ~2 tons of gold. Overall, the total outcrop area of the YHF is $\sim 6.2 \times 10^5\ m^2$ and the total mass is $\sim 7.5 \times 10^6$ tons, including $\sim 7.5 \times 10^5$ tons of Cu and Zn and ~18 tons of gold (Table 3).

It is well known that SMS mounds exhibit vertical mineralization zonation features (Knott et al., 1998). Murton et al. (2019) proposed an approximately 100-m-thick underlying stockwork zone in the TAG eSMS mounds using geophysical data. Similarly, a quartz-pyrite stockwork zone was located 45–100 m below the seafloor of the TAG active mound, accounting for ~30% of the total mass, while a sulfide-breccia complex was located in the top 45 m of the mound (Hannington et al., 1998). Based on the TAG active mound's data, the total YHF resources could reach 10.6×10^6 tons, including the stockwork zone. In addition, recent shallow drilling results found massive sulfides beneath the sediments, but they could not be distinguished at the surface of the seafloor; if some hydrothermal sediment regions have underlying massive sulfides, then the maximum total mass could be $\sim 45.1 \times 10^6$ tons.

5.3. Comparisons to other hydrothermal fields

Previous studies have estimated the resources of several large SMS deposits in the global oceans. Metalliferous submarine sediments of the Atlantis-II-Deep deposit in the Red Sea contain $\sim 4.25 \times 10^5$ tons of Cu and $\sim 1.89 \times 10^6$ tons of Zn (Guney et al., 1988). The estimated reserves of the Solwara-1 deposit in the Bismarck Sea are $\sim 1.54 \times 10^6$ tons (Lipton, 2008). The resources of Bent Hill field in the Middle Valley are $\sim 8.8 \times 10^6$ tons (Zierenberg et al., 1998), and a total mass of $\sim 1.2 \times 10^6$ tons is stored within the active vent fields along the Endeavour Segment of the Juan de Fuca Ridge (Jamieson et al., 2014). On a slow-spreading ridge, the ODP results revealed that the active mound of the TAG hydrothermal field harbors approximately 2.7×10^6 tons of massive sulfides and 1.2×10^6 tons of stockwork ore (Hannington et al., 1998).

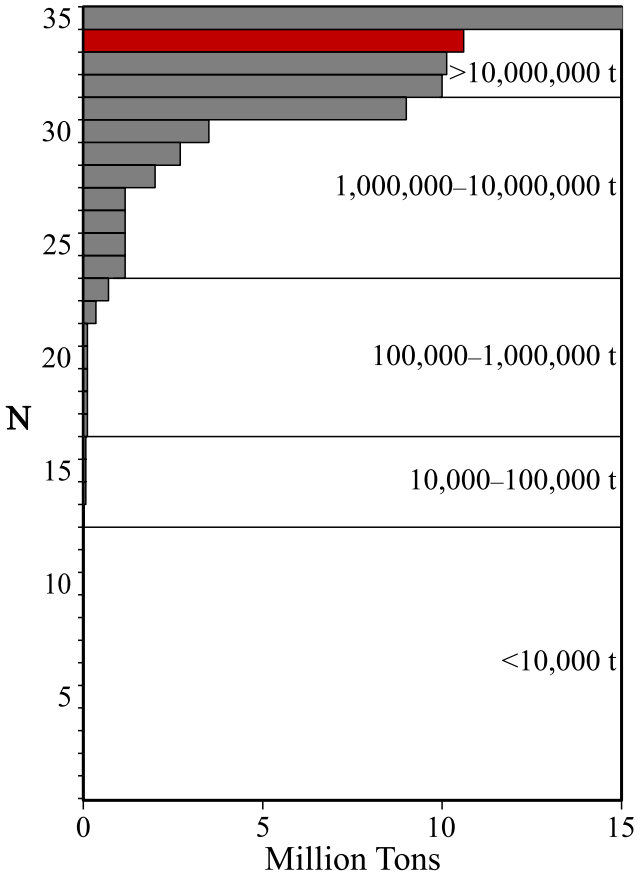

Fig. 5. The tonnages for 35 typical SMS deposits listed in Table 4. The YHF is denoted with a red bar. The largest deposit (~26 Mt) includes the 5 TAG eSMS mounds (Murton et al., 2019).

Table 4
Estimated sizes of 35 typical SMS deposits from different mid-ocean ridges. The size of each deposit is estimated using the outcrop area vs. tonnage relationship from Hannington et al. (2010), except for the YHF and the TAG active mound, and the TAG eSMS mounds. References: 1. Chen et al. (2018), 2. Hannington et al. (2011), 3. Hannington et al. (1998), 4. Murton et al. (2019), and 5. Cherkashov et al. (2010).

Site	Spreading Rate (mm/yr)	Setting	Activity	Outcrop Area (m^2)	Estimated Size (tones)	Ref
Southwest Indian Ridge						
Yuhuang-1,	14	MORB/ Ultramafic	Inactive	619,006	10,650,000–45,100,000	This study
Tianzuo	14	Ultramafic	Inactive	434,000	>3,000,000	1
Mt. Jourdanne	14	MORB	Inactive	<100	<3000	2
Mid-Atlantic Ridge						
Rainbow Field	21	Ultramafic	Active	30,000	300,000–1,000,000	2
Broken Spur	23	MORB	Active	5000	100,000–300,000	2
TAG active mound	24	MORB	Active	30,000	3,900,000	3
TAG eSMS mounds	24	MORB	Inactive	--	17,000,000–66,000,000	4
Alvin Zone	24	MORB	Inactive	100,000	2,000,000	2
MIR Zone	24	MORB	Inactive	>50,000	1,000,000–3,000,000	2
Snakepit Field	24	MORB	Active	15,000	100,000–300,000	2
Zenith-Victory	26	MORB	Inactive	–	10,000,000	5
13°30′N Semyenov	26	MORB	Inactive	>300,000	9,000,000	5
Krasnov	26	MORB	Active/ Inactive	150,000	>3,000,000	5
Ashadze 1	26	Ultramafic	Active/ Inactive	>50,000	1,000,000–3,000,000	2
Ashadze 2	26	Ultramafic	Active/ Inactive	>50,000	1,000,000–3,000,000	2
Logatchev 1	26	Ultramafic	Active/ Inactive	>5000	100,000–300,000	2
Logatchev 2	26	Ultramafic	Active /Inactive	1000	10,000–30,000	2
5°S, Turtle Pits	36	MORB	Active	5000	100,000–300,000	2
Central Indian Ridge						
JX/MESO Zone	45	MORB	Inactive	>50,000	1,000,000–3,000,000	2
Edmond Field	46	MORB	Active	3000	30,000–100,000	2
Kairei Field	48	MORB	Active	3000	30,000–100,000	2
Juan de Fuca Ridge						
CoAxial Site	56	MORB	Active	<100	<3000	2
North Cleft	56	MORB	Active	<100	<3000	2
South Cleft	56	MORB	Active	<100	<3000	2
Axial Seamount	56	MORB	Active	<100	<3000	2
Endeavour Ridge						
Main Field	57	MORB	Active	5000	100,000–300,000	2
Mothra	57	MORB	Active	5000	100,000–300,000	2
High-Rise	57	MORB	Active	3,000	30,000–100,000	2
Clam Bed	57	MORB	Active	<100	<3000	2
East Pacific Rise						
21°N	92	MORB	Active	<100	<3000	2
12°50′N	105	MORB	Active	5000	100,000–300,000	2
11°30′N	107	MORB	Active	<100	<3000	2
7°24′S	137	MORB	Active	<100	<3000	2
17°26′S	146	MORB	Active	<100	<3000	2
22°30′S	149	MORB	Active	<100	<3000	2

Recent investigations by the Blue Mining Project calculated the mineral resources of the TAG eSMS mounds at 17–66 × 10^6 tons (Murton et al., 2019). Using a Monte Carlo simulation, Juliani and Ellefmo (2018) calculated the total amount of metal reserves on the ultraslow-spreading Mohns Ridge to be 447,000 tons.

The tonnage of the SMS deposits from the different mid-ocean ridges indicates that the YHF ranks in the top of 35 typical SMS deposits described worldwide (Fig. 5). Furthermore, most deposits with >1 million tons are preserved in slow- and ultraslow-spreading ridges (Table 4), for which the spreading rates are ~20–55 mm/yr and <20 mm/yr (Dick et al., 2003). The evolution of hydrothermal systems on the slow- and ultraslow-spreading ridges is primarily tectonically controlled (German and Parson, 1998; Gràcia et al., 2000; Parson et al., 2000). The development of long-lived detachment faults makes the oceanic crust unusually thin, and therefore, improves its permeability, enabling seawater to penetrate deeply and facilitating continuous serpentinization with ultramafic rocks, given the availability of a heat source (German et al., 2016; Von Damn, 2000). Therefore, hydrothermal activity can last for a very long time, and tectonic-hosted deposits (e.g., the YHF) are more favorable for the accumulation of sulfides. Moreover, detachment fault-related hydrothermal systems generally form sulfide mineralization belt along or across the striking direction. For instance, five sulfide districts were identified in the Semyenov field on an oceanic core complex (Cherkashov et al., 2010); and several hydrothermal activities have been observed recently adjacent to the active mound in the TAG field during detailed survey conducted by the Blue Mining Project (Murton et al., 2019). Due to the lack of the detailed investigation in the YHF, more sulfide resources may be discovered during future exploration, and hence the YHF has the potential to be the largest field on the sediment-free mid-ocean ridges.

Compared to the SMS deposits in the largest size class (Hannington et al., 2010), the amount of Cu in the SWS, NES, and total YHF is found to surpass most deposits (Fig. 6), with the addition of over 5.2 × 10^5 tons of Zn and ~18 tons of Au. As a result, the YHF is one of the largest SMS deposits worldwide. However, due to differing degrees of investigation, most large deposits on mid-ocean ridges have been found on the slow-spreading MAR (Table 4). Radioisotope dating of the sulfide minerals of other hydrothermal fields (e.g., the Duanqiao-1 field at 0.7–84 kyr and the Mt. Jourdanne field at 13–70 kyr) on the SWIR revealed similar ages of hydrothermal activity (Münch et al., 2001; Yang et al., 2017), which are older than those of the TAG hydrothermal field (5–10 kyr; Hannington et al., 1998), but younger than those of the 18 hydrothermal fields along the Northern Equatorial MAR (~66 kyr on average; Cherkashov et al., 2017). Usually, the longer the hydrothermal activity lasts, the more the sulfide accumulates; therefore, the scales of these deposits may be larger than the TAG active mound (3.9 × 10^6 tons), and a slightly smaller than the fields along the Northern Equatorial MAR (e.g., Zenith-Victory, 10 × 10^6 tons; Semyenov, 9 × 10^6 tons; Table 4). Therefore, our results suggest that the ultraslow-spreading SWIR has a high potential to form large-scale sulfide deposits.

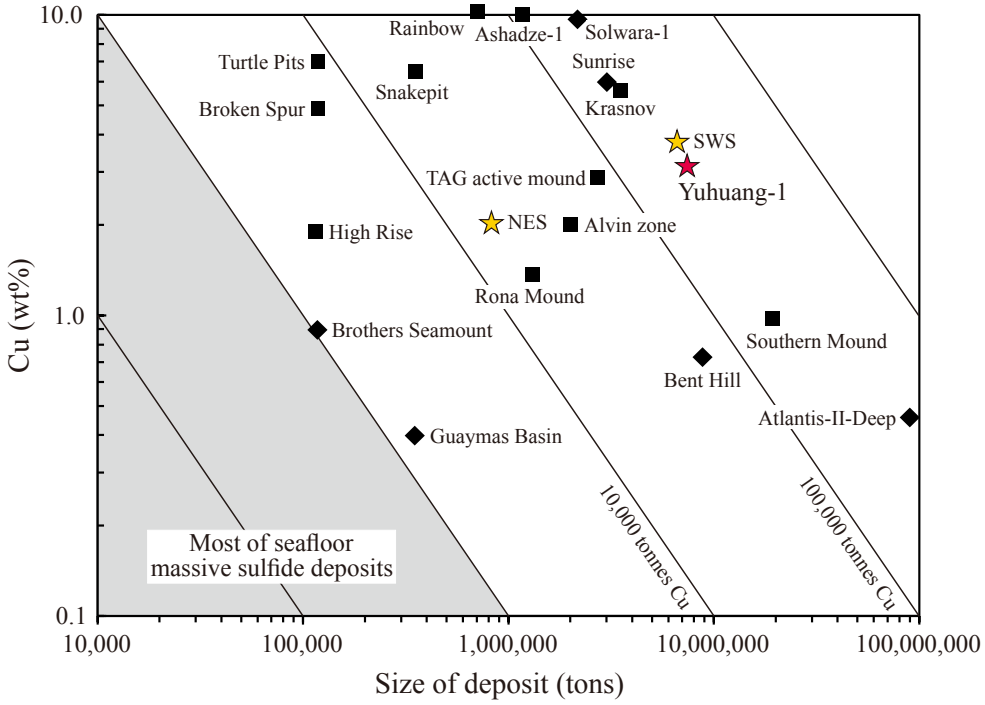

Fig. 6. The grade-tonnage plot for Cu in the largest deposits, modified from Hannington et al. (1998), Hannington et al. (2010). The data for the NES, SWS and the total YHF are presented in Tables 2 and 3, and are shown by the yellow and red stars, respectively. Data for most deposits are obtained from Hannington et al. (2010), Hannington et al. (2011) and the references therein, except for the case of the TAG active mound (Hannington et al., 1998), the Southern mound, and the Rona mound (Murton et al., 2019), the Atlantis-II-Deep (Guney et al., 1988), Bent Hill (Zierenberg et al., 1998), and High Rise (Jamieson et al., 2014). The deposits on the mid-ocean ridges are denoted with black squares, whereas the deposits in the remaining tectonic settings are denoted using black diamonds.

6. Conclusions

According to seafloor observations and sampling, the YHF is composed of two sulfide-rich areas, the SWS and NES, and three types of hydrothermal precipitates, i.e., sulfide-rich mounds, sulfide-rich breccia, and hydrothermal sediment. The absence of venting or vent-endemic species, the lack of active chimneys, and extensive oxidation and collapse, taken together, indicate that the mounds of YHF are likely extinct.

The total estimated resources of the YHF are ~10.6 × 10^6 tons including the stockwork zone, with at least 7.5 × 10^5 tons of Cu and Zn and ~18 tons of Au. In addition, the surface of the YHF is generally covered by a layer of hydrothermal sediments mixed with sulfide-rich breccias, which may have underlying massive sulfides; therefore, the total mass may be much larger, up to ~45.1 × 10^6 tons. Accordingly, this study suggests that the YHF is one of the largest SMS deposits worldwide and that ultraslow-spreading ridges have the best prospect for exploration of the large-scale sulfide deposits.

Declaration of Competing Interest

The authors declare that they have no known competing financial interests or personal relationships that could have appeared to influence the work reported in this paper.

Acknowledgements

This study was financially supported by the National Key R&D Program of China (2018YFC0309900, 2017YFC0306603 and 2017YFC0306203), Natural Science Foundation of China (42006074, 42073010, and 41806076), Natural Science Foundation of Zhejiang Province (LQ19D060002), China Ocean Mineral Resources R & D Association Project (DY135-S1-1-02), and Macao Science and Technology Development Fund (FDCT-002/2018/A1). We thank the captains and crews of the Chinese Dayang cruises.

Appendix A. Supplementary data

Supplementary data to this article can be found online at https://doi.org/10.1016/j.oregeorev.2021.104169.

References

Baker, E.T., German, C.R., 2004. In: On the Global Distribution of Hydrothermal Vent Fields. Geophysical Monograph Series. American Geophysical Union, Washington DC, pp. 245–266.
Beaulieu, S.E., Baker, E.T., German, C.R., 2015. Where are the undiscovered hydrothermal vents on oceanic spreading ridges? Deep Sea Res. Part II 121, 202–212.
Cannat, M., Rommevaux-Jestin, C., Sauter, D., Deplus, C., Mendel, V., 1999. Formation of the axial relief at the very slow spreading Southwest Indian Ridge (49° to 69°E). J. Geophys. Res. Solid Earth 104 (B10), 22825–22843.
Cannat, M., Sauter, D., Mendel, V., Ruellan, E., Okino, K., Escartin, J., Combier, V., Baala, M., 2006. Modes of seafloor generation at a melt-poor ultraslow-spreading ridge. Geology 34 (7), 605.
Chen, J., Tao, C., Liang, J., Liao, S., Dong, C., Li, H., Li, W., Wang, Y., Yue, X., He, Y., 2018. Newly discovered hydrothermal fields along the ultraslow-spreading Southwest Indian Ridge around 63°E. Acta Oceanol. Sin. 37 (11), 61–67.
Cherkashov, G., Beltenev, V., Ivanov, V., Lazareva, L., Samovarov, M., Shilov, V., Stepanova, T., Glasby, G.P., Kuznetsov, V., 2010. Seafloor massive sulfides from the northern equatorial mid-Atlantic Ridge: New discoveries and perspectives. Mar. Georesour. Geotechnol. 28 (3), 222–239.
Cherkashov, G., Kuznetsov, V., Kuksa, K., Tabuns, E., Maksimov, F., Bel'tenev, V., 2017. Sulfide geochronology along the Northern Equatorial mid-Atlantic Ridge. Ore Geol. Rev. 87, 147–154.
Dias, Á.S., Barriga, F.J.A.S., 2006. Mineralogy and geochemistry of hydrothermal sediments from the serpentinite-hosted Saldanha hydrothermal field (36°34′N; 33°26′W) at MAR. Mar. Geol. 225 (1–4), 157–175.
Dick, H.J.B., Lin, J., Schouten, H., 2003. An ultraslow-spreading class of ocean ridge. Nature 426 (6965), 405–412.
Fouquet, Y., Cambon, P., Etoubleau, J., Charlou, J.L., OndréAs, H., Barriga, F.J.A.S., Cherkashov, G., Semkova, T., Poroshina, I., Bohn, M., Donval, J.P., Henry, K., Murphy, P., Rouxel, O., 2010. Geodiversity of hydrothermal processes along the mid-Atlantic Ridge–ultramafic-hosted mineralization: A new type of oceanic Cu-Zn-Co-Au volcanogenic massive sulfide deposit. In: Rona, P.A., Devey, C.W., Dyment, J., Murton, B.J. (Eds.), Diversity of Hydrothermal Systems on Slow Spreading Ocean Ridges. American Geophysical Union, Washington DC, p. 440.
Georgen, J.E., Lin, J., Dick, H.J.B., 2001. Evidence from gravity anomalies for interactions of the Marion and Bouvet hotspots with the Southwest Indian Ridge: Effects of transform offsets. Earth Planet. Sci. Lett. 187 (3–4), 283–300.
German, C.R., Parson, L.M., 1998. Distributions of hydrothermal activity along the mid-Atlantic Ridge: Interplay of magmatic and tectonic controls. Earth Planet. Sci. Lett. 160 (3–4), 327–341.

German, C.R., Petersen, S., Hannington, M.D., 2016. Hydrothermal exploration of mid-ocean ridges: Where might the largest sulfide deposits be forming? Chem. Geol. 420, 114–126.

Graber, S., Petersen, S., Yeo, I., Szitkar, F., Klischies, M., Jamieson, J., Hannington, M.D., Rothenbeck, M., Wenzlaff, E., Augustin, N., Stobbs, I., 2020. Structural control, evolution, and accumulation rates of massive sulfides in the TAG hydrothermal field. Geochem. Geophys. Geosyst. 21 https://doi.org/10.1029/2020GC009185 e2020GC009185.

Gràcia, E., Charlou, J.L., Radford-Knoery, J.L., Parson, L.M., 2000. Non-transform offsets along the mid-Atlantic Ridge south of the Azores (38°N–34°N): Ultramafic exposures and hosting of hydrothermal vents. Earth Planet. Sci. Lett. 177 (1–2), 89–103.

Guney, M., Al-Marhoun, M.A., Nawab, Z.A., 1988. Metalliferous sub-marine sediments of the Atlantis-II-Deep, Red Sea. Can. Inst. Min. Metall. Bull. 81, 33–39.

Haase, K.M., Koschinsky, A., Petersen, S., Devey, C.W., German, C., Lackschewitz, K.S., Melchert, B., Seifert, R., Borowski, C., Giere, O., Paulick, H., 2009. Diking, young volcanism and diffuse hydrothermal activity on the southern mid-Atlantic Ridge: The Lilliput field at 9°33′S. Mar. Geol. 266 (1–4), 52–64.

Hannington, M., Jamieson, J., Monecke, T., Petersen, S., 2010. Modern Sea-floor massive sulfides and base metal resources: Toward an estimate of global sea-floor massive sulfide potential. Soc. Econ. Geol. Special Publ. 15, 317–338.

Hannington, M., Jamieson, J., Monecke, T., Petersen, S., Beaulieu, S., 2011. The abundance of seafloor massive sulfide deposits. Geology 39 (12), 1155–1158.

Hannington, M.D., Galley, A.G., Herzig, P.M. and Petersen, S. 1998. Comparison of the TAG mound and stockwork complex with Cyprus-type massive sulfide deposits. In: Proceedings of the Ocean Drilling Program: Scientific Results, Herzig, P.M., Humphris, S.E., Miller, D.J., and Zierenberg, R.A. (Eds). College Station, TX: 389-415.

Humphris, S.E., Herzig, P.M., Miller, D.J., Alt, J.C., Becker, K., Brown, D., Brügmann, G., Chiba, H., Fouquet, Y., Gemmell, J.B., Guerin, G., Hannington, M.D., Holm, N.G., Honnorez, J.J., Iturrino, G.J., Knott, R., Ludwig, R., Nakamura, K., Petersen, S., Reysenbach, A., Rona, P.A., Smith, S., Sturz, A.A., Tivey, M.K., Zhao, X., 1995. The internal structure of an active sea-floor massive sulphide deposit. Nature 377 (6551), 713–716.

Jamieson, J.W., Clague, D.A., Hannington, M.D., 2014. Hydrothermal sulfide accumulation along the Endeavour Segment, Juan de Fuca Ridge. Earth Planet. Sci. Lett. 395, 136–148.

Juliani, C., Ellefmo, S.L., 2018. Resource assessment of undiscovered seafloor massive sulfide deposits on an Arctic Mid-Ocean Ridge: Application of grade and tonnage models. Ore Geol. Rev. 102, 818–828.

Knott, R., Fouquet, Y., Honnorez, J., Petersen, S. and Bohn, M. 1998. Petrology of hydrothermal mineralization: A vertical section through the TAG, Mound. In: Proceedings of the Ocean Drilling Program: Scientific Results, Herzig, P.M., Humphris, S.E., Miller, D.J., and Zierenberg, R.A. (Eds). College Station, TX: 5–26.

Li, J.B., Jian, H.C., Chen, Y.S.J., Singh, S.C., Ruan, A., Qiu, X.L., Zhao, M.H., Wang, X.G., Niu, X.G., Ni, J.Y., Zhang, J.Z., 2015. Seismic observation of an extremely magmatic accretion at the ultraslow spreading Southwest Indian Ridge. Geophys. Res. Lett. 42 (8), 2656–2663.

Liao, S., Tao, C., Li, H., Barriga, F.J.A.S., Liang, J., Yang, W., Yu, J., Zhu, C., 2018a. Bulk geochemistry, sulfur isotope characteristics of the Yuhuang-1 hydrothermal field on the ultraslow-spreading Southwest Indian Ridge. Ore Geol. Rev. 96, 13–27.

Liao, S., Tao, C., Zhu, C., Li, H., Li, X., Liang, J., Yang, W., Wang, Y., 2019a. Two episodes of sulfide mineralization at the Yuhuang-1 hydrothermal field on the Southwest Indian Ridge: Insight from Zn isotopes. Chem. Geol. 507, 54–63.

Liao, S., Tao, C., Li, H., Zhang, G., Liang, J., Yang, W., Wang, Y., 2018b. Surface sediment geochemistry and hydrothermal activity indicators in the Dragon Horn area on the Southwest Indian Ridge. Mar. Geol. 398, 22–34.

Liao, S., Tao, C., Dias, Á.A., Su, X., Yang, Z., Ni, J., Liang, J., Yang, W., Liu, J., Li, W., Dong, C. 2019b. Surface sediment composition and distribution of hydrothermal derived elements at the Duanqiao-1 hydrothermal field, Southwest Indian Ridge. Marine Geology, 416: http://www.ncbi.nlm.nih.gov/pubmed/ 105975.

Lipton, I. 2008. Mineral resource estimate, Solwara 1 project, Bismarck Sea, Papua New Guinea: NI43-101 Technical Report for Nautilus Minerals Inc. http://www.nautilusminerals.com/i/pdf/2008-02-01_Solwara1_43-101.pdf (July 2011).

Lusty, P.A.J., Murton, B.J., 2018. Deep-ocean mineral deposits: Metal resources and windows into earth processes. Elements 14 (5), 301–306.

Marques, A.F.A., Barriga, F.J.A.S., Chavagnac, V., Fouquet, Y., 2006. Mineralogy, geochemistry, and Nd isotope composition of the Rainbow hydrothermal field, mid-Atlantic Ridge. Miner. Deposita 41 (1), 52–67.

Münch, U., Lalou, C., Halbach, P., Fujimoto, H., 2001. Relict hydrothermal events along the super-slow Southwest Indian spreading ridge near 63°56′E — Mineralogy, chemistry and chronology of sulfide samples. Chem. Geol. 177 (3–4), 341–349.

Murton, B.J., Lehrmann, B., Dutrieux, A.M., Martins, S., de la Iglesia, A.G., Stobbs, I.J., Barriga, F.J.A.S., Bialas, J., Dannowski, A., Vardy, M.E., North, L.J., Yeo, I.A.L.M., Lusty, P.A.J., Petersen, S., 2019. Geological fate of seafloor massive sulphides at the TAG hydrothermal field (mid-Atlantic Ridge). Ore Geol. Rev. 107, 903–925.

Parson, L., Gràcia, E., Coller, D., German, C., Needham, D., 2000. Second-order segmentation; the relationship between volcanism and tectonism at the MAR, 38°N–35°40′N. Earth Planet. Sci. Lett. 178 (3–4), 231–251.

Petersen, S., Krätschell, A., Augustin, N., Jamieson, J., Hein, J.R., Hannington, M.D., 2016. News from the seabed – Geological characteristics and resource potential of deep-sea mineral resources. Marine Policy 70, 175–187.

Petersen, S., Kuhn, K., Kuhn, T., Augustin, N., Hékinian, R., Franz, L., Borowski, C., 2009. The geological setting of the ultramafic-hosted Logatchev hydrothermal field (14°45′N, mid-Atlantic Ridge) and its influence on massive sulfide formation. Lithos 112 (1–2), 40–56.

Sauter, D., Patriat, P., Rommevaux-Jestin, C., Cannat, M., Briais, A., 2001. The Southwest Indian Ridge between 49°15′E and 57°E: Focused accretion and magma redistribution. Earth Planet. Sci. Lett. 192 (3), 303–317.

Spagnoli, G., Jahn, A., Halbach, P., 2016. First results regarding the influence of mineralogy on the mechanical properties of seafloor massive sulfide samples. Eng. Geol. 214, 127–135.

Spiess, F.N., Macdonald, K.C., Atwater, T., Ballard, R., Carranza, A., Cordoba, D., Cox, C., Garcia, V.M., Francheteau, J., Guerrero, J., Hawkins, J., Haymon, R., Hessler, R., Juteau, T., Kastner, M., Larson, R., Luyendyk, B., Macdougall, J.D., Miller, S., Normark, W., Orcutt, J., Rangin, C., 1980. East Pacific Rise: Hot springs and geophysical experiments. Science 207 (4438), 1421–1433.

Tao, C., Li, H., Jin, X., Zhou, J., Wu, T., He, Y., Deng, X., Gu, C., Zhang, G., Liu, W., 2014. Seafloor hydrothermal activity and polymetallic sulfide exploration on the Southwest Indian Ridge. Chin. Sci. Bull. 59 (19), 2266–2276.

Tao, C., Lin, J., Guo, S., Chen, Y.J., Wu, G., Han, X., German, C.R., Yoerger, D.R., Zhou, N., Li, H., Su, X., Zhu, J., 2012. First active hydrothermal vents on an ultraslow-spreading center: Southwest Indian Ridge. Geology 40 (1), 47–50.

Tao, C., Seyfried, W.E., Lowell, R.P., Liu, Y., Liang, J., Guo, Z., Ding, K., Zhang, H., Liu, J., Qiu, L., Egorov, I., Liao, S., Zhao, M., Zhou, J., Deng, X., Li, H., Wang, H., Cai, W., Zhang, G., Zhou, H., Lin, J., Li, W., 2020. Deep high-temperature hydrothermal circulation in a detachment faulting system on the ultra-slow spreading ridge. Nat. Commun. 11 (1), 1300.

Tao, C., Wu, T., Jin, X., Dou, B., Li, H., Zhou, J., 2013. Petrophysical characteristics of rocks and sulfides from the SWIR hydrothermal field. Acta Oceanol. Sin. 32 (12), 118–125.

Tivey, M.K., Humphris, S.E., Thompson, G., Hannington, M.D., Rona, P.A., 1995. Deducing patterns of fluid flow and mixing within the TAG active hydrothermal mound using mineralogical and geochemical data. J. Geophys. Res. Solid Earth 100 (B7), 12527–12555.

Von Damn, K.L., 2000. Chemistry of hydrothermal vent fluids from 9°–10°N, East Pacific Rise: "Time zero", the immediate posteruptive period. J. Geophys. Res. Solid Earth 105 (B5), 11203–11222.

Yang, W., Tao, C., Li, H., Liang, J., Liao, S., Long, J., Ma, Z., Wang, L., 2017. 230Th/238U dating of hydrothermal sulfides from Duanqiao hydrothermal field, Southwest Indian Ridge. Mar. Geophys. Res. 38 (1–2), 71–83.

Yu, X., Dick, H.J.B., 2019. Plate-driven micro-hotspots and the evolution of the Dragon Flag melting anomaly, Southwest Indian Ridge. Earth Planet. Sci. Lett. 531, 116002 https://doi.org/10.1016/j.epsl.2019.116002.

Yu, Z., Gao, Y., Zhai, S., Liu, F., 2011. Resolving the hydrothermal signature by sequential leaching studies of sediments from the middle of the Okinawa Trough. Sci. China Earth Sci. 55 (4), 665–674 (In Chinese with English abstract).

Zhu, C., Tao, C., Yin, R., Liao, S., Yang, W., Liu, J., Barriga, F.J.A.S., 2020a. Seawater versus mantle sources of mercury in sulfide-rich seafloor hydrothermal systems, Southwest Indian Ridge. Geochim. Cosmochim. Acta 281, 91–101.

Zhu, Z., Tao, C., Shen, J., Revil, A., Deng, X., Liao, S., Zhou, J., Wang, W., Nie, Z., Yu, J., 2020b. Self-potential tomography of a deep-sea polymetallic sulfide deposit on Southwest Indian Ridge. J. Geophys. Res. Solid Earth 125 (11). https://doi.org/10.1029/2020JB019738 e2020JB019738.

Zierenberg, R.A., Fouquet, Y., Miller, D.J., Bahr, J.M., Baker, P.A., Bjerkgård, T., Brunner, C.A., Duckworth, R.C., Gable, R., Gieskes, J., Goodfellow, W.D., Gröschel-Becker, H.M., Guèrin, G., Ishibashi, J., Iturrino, G., James, R.H., Lackschewitz, K.S., Marquez, L.L., Nehlig, P., Peter, J.M., Rigsby, C.A., Schultheiss, P., Shanks, W.C., Simoneit, B.R.T., Summit, M., Teagle, D.A.H., Urbat, M., Zuffa, G.G., 1998. The deep structure of a sea-floor hydrothermal deposit. Nature 392 (6675), 485–488.